COMPDYN 2013
4th ECCOMAS Thematic Conference on
Computational Methods in Structural Dynamics and Earthquake Engineering
M. Papadrakakis, V. Papadopoulos, V. Plevris (eds.)
Kos Island, Greece, 12–14 June 2013

# A SHEET PILING WALL AS A WAVE BARRIER FOR TRAIN INDUCED VIBRATIONS

**A. Dijckmans[1], A. Ekblad[2], A. Smekal[2], G. Degrande[1] and G. Lombaert[1]**

[1]KU Leuven Department of Civil Engineering
Kasteelpark Arenberg 40, B-3001 Leuven, Belgium
e-mail: {arne.dijckmans,geert.degrande,geert.lombaert}@bwk.kuleuven.be

[2] Trafikverket
405 33 Göteborg, Sweden
e-mail: {alf.ekblad,alexander.smekal}@trafikverket.se

**Keywords:** ground borne vibration, buried wall barrier, 2.5D, finite element, boundary element

**Abstract.** *Numerical simulations have been carried out with a two-and-a-half dimensional coupled finite element - boundary element methodology to assess the effectiveness of a sheet piling wall to reduce railway induced vibrations. In the method, the geometry of the problem is assumed invariant in the longitudinal direction along the track.*

*The sheet piling wall acts as a stiff wave barrier of which the effectiveness is determined by the depth and the contrast in stiffness between the barrier and the soil. It is important to take into account the orthotropic behavior of the sheet piling wall, as the bending stiffness in the vertical direction (along the profiles) is much larger than the bending stiffness in the longitudinal direction (perpendicular to the profiles). Calculations show that the reduction of vibration levels is entirely due to the relatively high axial stiffness and vertical bending stiffness, while the longitudinal bending stiffness is too low to affect the transmission of vibrations.*

*At Furet, Sweden, a sheet piling wall has been installed next to the track to reduce train induced vibrations in several buildings close to the track. The vibration levels caused by train passages have been measured before and after the construction of wall. Furthermore, the Rolling Stiffness Measurement Vehicle (RSMV) has been used to perform measurements with stationary track excitation. A preliminary comparison is made of the experimental results and predicted insertion loss values.*

## 1 INTRODUCTION

At Furet vibration problems occur in several buildings close to a railway track (Figure 1a). The site of Furet is located in the southwest of Sweden in the city of Halmstad along the West Coast Line between Gothenburg and Lund. The buildings in Furet have two to three floors and are mostly built around 1950, along $750\,\mathrm{m}$ at the west side of the track, $700\,\mathrm{m}$ north of Halmstad station. The track consists of a classical ballasted track.

In 2002 an Environmental court decided that residents should have less than $1.0\,\mathrm{mm/s}$ frequency weighted RMS at night (10pm-07am). Measurements indicate that in at least eight buildings the vibration levels exceed this value. The highest vibration levels were measured in the frequency range $4 - 5\,\mathrm{Hz}$.

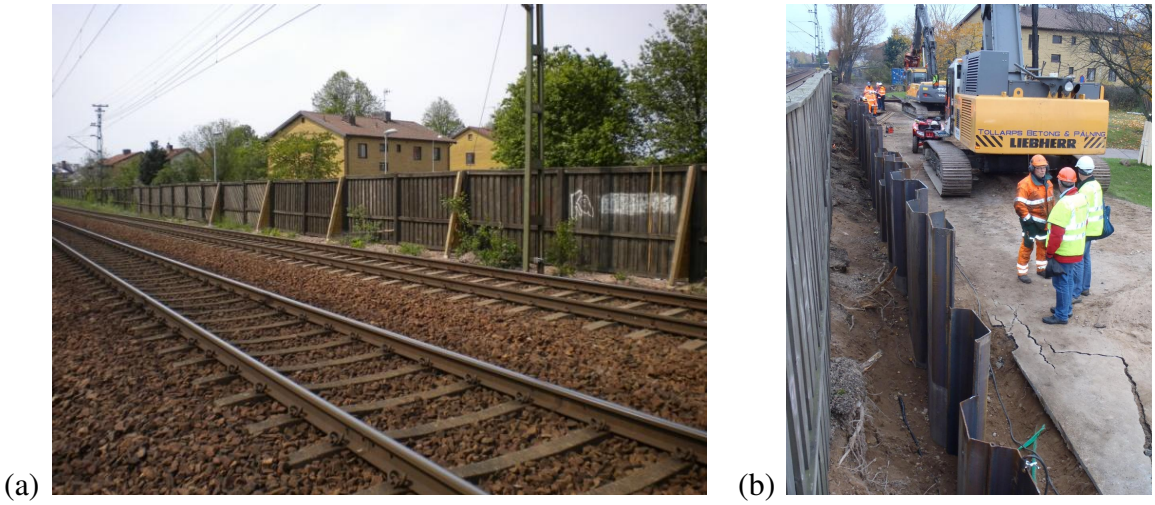


Figure 1: Site of Furet: (a) track, noise barrier and buildings close to the track, and (b) installation of the sheet piling wall.

The first attempt to mitigate vibration has been done in 2006. Sleepers at the track close to the noise barrier have been replaced and substituted by sleepers with under sleeper pads (USP). At the same time the ballast has been exchanged and leveling of the track has been carried out. Unfortunately measurements performed after these measures showed insufficient vibration mitigation. Therefore it was decided to use a sheet piling wall as a method to further reduce the train induced vibrations at the site. A sheet piling wall with a length of $100\,\mathrm{m}$ was installed next to the track in November 2011 (Figure 1b).

The sheet piling wall is a VL 603-K profile (Figure 2). The depth of the sheet piles is $12\,\mathrm{m}$ with every fourth pile extended to $18\,\mathrm{m}$. Adjacent sheet piles were welded together over the top $30\,\mathrm{cm}$. The distance from the center of the nearest track to the center of the sheet piling wall is approximately $5.60\,\mathrm{m}$. The properties of the VL 603-K profile are given in Table 1.

Measurements after installation of the sheet pile wall have showed sufficient reduction of vibration levels, except for a small house with wooden structure at approximately $40\,\mathrm{m}$ distance from the track.

The sheet piling wall designed and constructed by Trafikverket is subjected to a program of measurements and theoretical analysis within the frame of the EU FP7 project RIVAS (Railway Induced Vibration Abatement Solutions). First simulation results and experimental results are presented in this paper.

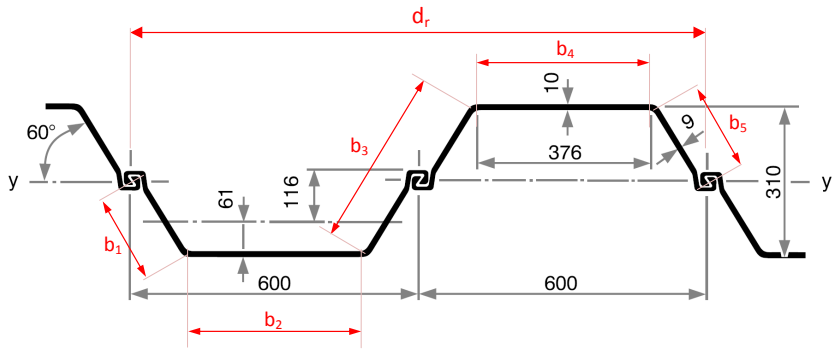


Figure 2: Cross section of the sheet piling wall (VL 603-K profile)

| Mass $m_{\mathrm{w}}$ $[\mathrm{kg/m^2}]$ | Sectional area $A_{\mathrm{w}}$ $[\mathrm{cm^2/m}]$ | Moment of inertia $I_{\mathrm{w}}$ $[\mathrm{cm^4/m}]$ | Width $t_{\mathrm{w}}$ $[\mathrm{m}]$ |
|---|---|---|---|
| 113.5 | 144.8 | 18900 | 0.310 |

Table 1: Characteristics of the sheet piling wall (VL 603-K profile)

## 2 MEASUREMENTS

### 2.1 Dynamic soil characteristics

Geotechnical and geophysical surveys performed by the consulting company Tyréns in the area include cone penetration tests (CPT), seismic cone penetration tests (SCPT), standard piston sampling, sampling by Helical auger and weight sounding. The undrained shear strength is $20-35\,\mathrm{kPa}$ to $13\,\mathrm{m}$ depth and $50-70\,\mathrm{kPa}$ deeper than $13\,\mathrm{m}$, investigation done in 4 boreholes with depth to at least $18\,\mathrm{m}$.

The soil profile consists of a relatively firm layer of sand up to $2-3\,\mathrm{m}$ depth underlain by clayey silt up to a depth of $5-10\,\mathrm{m}$ (layers of clay), underlain by silty clay. The silt has a density of $1850\,\mathrm{kg/m^3}$ and the clay $1710\,\mathrm{kg/m^3}$. These densities are determined as average values from three samples per meter from one of the boreholes.

The shear wave velocity $C_{\mathrm{s}}$ has been measured by means of a SCPT and multichannel analysis of surface waves (MASW) test. The SCPT test indicated a shear wave velocity of $110\,\mathrm{m/s}$ between $3-14\,\mathrm{m}$, and $150\,\mathrm{m/s}$ between $15-18\,\mathrm{m}$. Two setups were used for the MASW test. The first setup employed 24 geophones in a straight line perpendicular to the track, equally spaced between $10\,\mathrm{m}$ and $56\,\mathrm{m}$ from the hand-held hammer impact aluminium plate. The second setup used 24 geophones in a straight line perpendicular to the track, equally spaced between $10\,\mathrm{m}$ and $33\,\mathrm{m}$ from the hand-held hammer impact aluminium plate. The analysis shows a $2\,\mathrm{m}$ thick top layer with a shear wave velocity of $160\,\mathrm{m/s}$, a $10\,\mathrm{m}$ thick mid layer with a shear wave velocity of $115\,\mathrm{m/s}$ and a halfspace with a shear wave velocity of about $200\,\mathrm{m/s}$.

The results from the different in situ tests are in good agreement. The SCPT results showed a shear wave velocity of $110\,\mathrm{m/s}$ for the mid layer and a shear wave velocity of $150\,\mathrm{m/s}$ for the halfspace. The MASW results showed a slightly higher shear wave velocity, $119\,\mathrm{m/s}$ and $200\,\mathrm{m/s}$. The presence of the stiffer top layer impedes the determination of the dilatational wave velocity $C_{\mathrm{p}}$ from a seismic refraction test, the values for $C_{\mathrm{p}}$ have been estimated from the results for $C_{\mathrm{s}}$ assuming a Poisson's ratio of $0.40$. Table 2 provides a summary of the soil

parameters for each layer.

| Layer | Thickness $h$ [m] | Shear wave velocity $C_\mathrm{s}$ [m/s] | Dilatational wave velocity $C_\mathrm{p}$ [m/s] | Damping ratio $\beta$ [-] | Density $\rho$ [kg/m$^3$] | Poisson's ratio $\nu$ [-] |
|---|---|---|---|---|---|---|
| 1 | 2 | 154 | 375 | 0.025 | 1800 | 0.40 |
| 2 | 10 | 119 | 290 | 0.025 | 1850 | 0.40 |
| 3 | $\infty$ | 200 | 490 | 0.025 | 1710 | 0.40 |

Table 2: Dynamic soil characteristics for the Furet test site.

## 2.2 Vibration measurements

Vibration measurements were performed according to the RIVAS measurement protocol [1]. In the protocol, the combination of two procedures is recommended to determine the efficiency of vibration mitigation measures. In the first procedure, the vibration levels obtained at adjacent track sections with and without mitigation measure are compared to determine the insertion loss. In the second procedure, vibration levels before and after installation of the mitigation measure are compared.

At Furet, vibration measurements were performed both before and after installation of the sheet pile wall on two measurement lines perpendicular to the track, one at the test section with sheet pile wall and one at a reference section. Measurement line A was close to the middle of the sheet pile wall (Figure 3). Geophones were placed at $8\,\mathrm{m}$, $16\,\mathrm{m}$, $32\,\mathrm{m}$ and $64\,\mathrm{m}$ from the center of the track. Geophones were also placed at $8\,\mathrm{m}$ and $16\,\mathrm{m}$ at the opposite side of the track to verify whether there is no increase in vibration levels. Two geophones were placed on the sleepers to measure the track stiffness. A second, reference measurement line was placed a couple of hundred meters south of the sheet piling wall. Here, measurements were performed on the sleepers and at $8\,\mathrm{m}$ and $16\,\mathrm{m}$ from the track center.

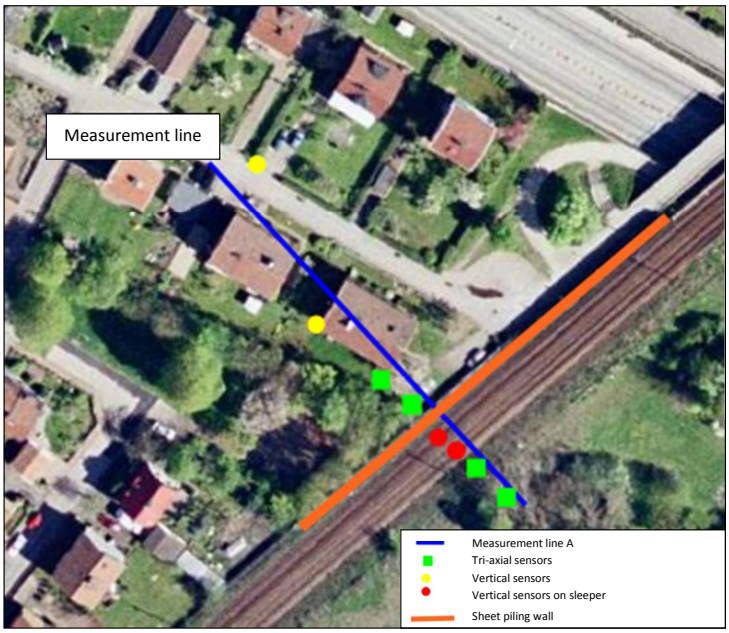


Figure 3: Measurement setup for the vibration measurements at the test site.

Vibration measurements during train passages have been performed during an entire week to include all types of traffic and to cover differences between working days and weekend days. At the test site, a total of 112 train passages occur per 24 hours, of which 29 are freight trains.

Preliminary comparison between the results at the test section before and after installation of the sheet pile wall indicate a significant reduction in vertical vibration levels behind the sheet pile wall at $8\,\mathrm{m}$, $16\,\mathrm{m}$, and $32\,\mathrm{m}$ from the track center. The effectiveness is higher closer to the wall where the maximum vibration levels are reduced by about $50\%$. At $32\,\mathrm{m}$ the maximum levels are reduced by about $30\%$. At $64\,\mathrm{m}$ from the track center, no reduction in maximum vibration levels is seen. Measurements at the other side of the track show no increase in vertical vibration levels.

Furthermore, vibration measurements have been carried out with the Rolling Stiffness Measurement Vehicle (RSMV). In this case stationary excitation of the track has been applied. The excitation has been performed before and after installation of the sheet pile wall at both the test site and the reference site. The excitation duration was $30$ seconds at each operating frequency ($3\,\mathrm{Hz}$, $4\,\mathrm{Hz}$, $5\,\mathrm{Hz}$, $6\,\mathrm{Hz}$, $7\,\mathrm{Hz}$, $8\,\mathrm{Hz}$, $9\,\mathrm{Hz}$, $10\,\mathrm{Hz}$, $15\,\mathrm{Hz}$ and $20\,\mathrm{Hz}$). Figure 4 shows preliminary results for the measured insertion loss for the excitation frequencies of $5\,\mathrm{Hz}$ and $20\,\mathrm{Hz}$, as determined from the measurements at the test site before and after installation of the sheet pile wall. These results indicate that a considerable reduction is already obtained at $5\,\mathrm{Hz}$. Furthermore, the reduction generally decreases with increasing distance from the sheet piling wall.

Further processing of the measurements is needed for a more detailed assessment of the effectiveness.

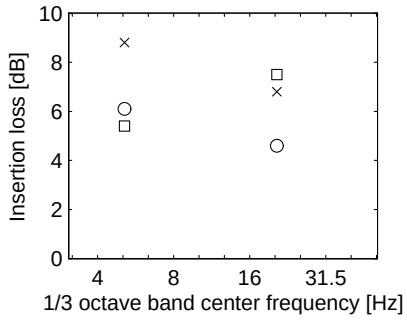


Figure 4: Vertical insertion loss measured at $8\,\mathrm{m}$ ($\times$), $16\,\mathrm{m}$ ($\square$) and $32\,\mathrm{m}$ ($\circ$) with stationary track excitation (RSMV) at $5\,\mathrm{Hz}$ and $20\,\mathrm{Hz}$.

## 3 SIMULATIONS

### 3.1 Methodology

For the prediction of railway induced vibrations, the geometry of the track-soil system is often assumed to be invariant in the longitudinal direction. The loading due to a point force or train introduces a dependence on the longitudinal dimension. By assuming homogeneity of the geometry and material properties in the track direction, a Fourier transform of the longitudinal coordinate allows for a two-and-half-dimensional (2.5D) approach [2, 3, 4]. This method is computationally more efficient than a full 3D approach. Andersen and Nielsen [5] have applied the methodology to study the effect of vibration isolating screens along a railway track.

For the computation of the dynamic interaction between a layered soil and structures with a longitudinally invariant geometry, a coupled finite element - boundary element (FE–BE)

methodology formulated in the frequency domain is used [6]. The classical 2.5D FE method is combined with the 2.5D BE method using 2.5D Green's functions of a horizontally layered halfspace [7, 8]. In this way, the free surface and the layer interfaces of the halfspace don't have to be discretized with boundary elements, avoiding spurious reflections at mesh truncations. The BE mesh can be limited to the interface between the structure and the soil, significantly reducing the size of the BE mesh.

Solving the set op coupled FE–BE equations provides the structural response in the frequency-wavenumber domain. The radiated wavefield in the soil is obtained by means of the wavenumber domain formulation of the integral representation theorem [6]. Finally, an inverse Fourier transform is used to recover the three-dimensional response in the frequency-spatial domain.

### 3.2 Sheet piling wall model

The sheet piling wall was analyzed by means of 2.5D calculations. Since this requires assuming the geometry of the sheet piling wall to be longitudinally invariant, separate calculations have been made for depths $d$ of 12 m and 18 m. The actual sheet piles have a depth of 12 m, with every fourth sheet pile extended to 18 m. To reduce the computational cost, the presence of the track was disregarded in the models. A vertical unit harmonic point force is applied directly at the surface at a distance $R = 5.60\,\mathrm{m}$ from the sheet pile wall (Figure 5). This corresponds with the distance from the center of the nearest track to the center of the sheet piling wall at the test site in Furet.

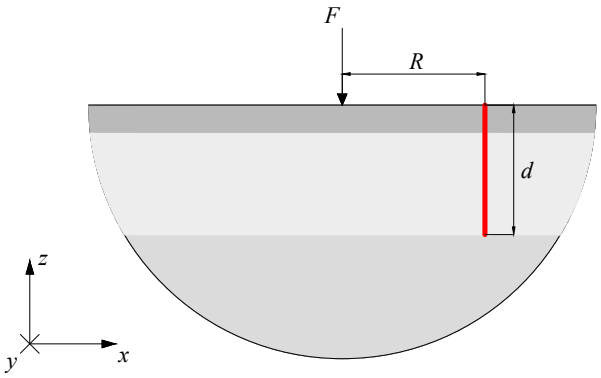


Figure 5: 2.5D plate model of the sheet piling wall

An equivalent orthotropic plate model of the sheet piling wall was adopted in the calculations to account for the fact that the stiffness is much larger for bending with respect to the horizontal axis than for the vertical axis. In the frequency range of interest (0-100 Hz), the bending wavelength $\lambda_\mathrm{b}$ in the sheet piling wall is much larger than the repetition distance $d_\mathrm{r} = 1200\,\mathrm{mm}$ of the sheet piling wall. Therefore, the profiling of the plate can be disregarded and the sheet piling wall can be modeled as an equivalent orthotropic plate.

The thickness $\bar{t}$, moduli of elasticity $\bar{E}_y$ and $\bar{E}_z$, and Poisson's ratios $\bar{\nu}_{yz}$ and $\bar{\nu}_{zy}$ of the equivalent orthotropic plate are chosen such that the plate has approximately the same bending stiffness as well as axial stiffness as the VL 603-K profile. The axial stiffness and bending stiffness in the vertical direction can be determined from the characteristics of the VL 603-K profile (Table 1).

$$\frac{\bar{E}_z \bar{t}}{1 - \bar{\nu}_{yz}\bar{\nu}_{zy}} = E_\mathrm{s} A_\mathrm{w} = 3.041 \times 10^9\,\mathrm{N/m} \tag{1}$$

$$\frac{\bar{E}_z \bar{t}^3}{12(1-\bar{\nu}_{yz}\bar{\nu}_{zy})} = E_\mathrm{s} I_\mathrm{w} = 3.97 \times 10^7 \,\mathrm{Nm^2/m} \tag{2}$$

with $E_\mathrm{s} = 210\,\mathrm{GPa}$ the modulus of elasticity of steel. Solving equations (1) and (2) yields $\bar{t} = 0.396\,\mathrm{m}$ and $\frac{\bar{E}_z}{1-\bar{\nu}_{zy}\bar{\nu}_{yz}} = 7.68\,\mathrm{GPa}$. Due to the profiling of the sheet piling wall, the Poisson's ratios $\bar{\nu}_{yz}$ and $\bar{\nu}_{zy}$ can be assumed zero. This eventually gives a modulus of elasticity $\bar{E}_z = 7.68\,\mathrm{GPa}$.

The bending stiffness in the longitudinal direction is approximately the same as this of a flat steel plate with the same thickness, but taking into account the effective increase in plate width due to the profiles [9].

$$\frac{\bar{E}_y \bar{t}^3}{12(1-\bar{\nu}_{yz}\bar{\nu}_{zy})} = \frac{E_\mathrm{s} h^3}{12(1-\nu_\mathrm{s}^2)} \frac{d_\mathrm{r}}{\sum b_n} = 1.27 \times 10^4 \,\mathrm{Nm^2/m} \tag{3}$$

with $\nu_\mathrm{s} = 0.30$ the Poisson's ratio of steel, $h = 9\,\mathrm{mm}$ the thickness of the steel plate and $\sum b_n = 1320\,\mathrm{mm}$ the total length of the sheet piling wall profile along the length $d_\mathrm{r} = 1200\,\mathrm{mm}$ (Figure 2). Solving for the longitudinal modulus of elasticity yields a value $\bar{E}_y = 2.47\,\mathrm{MPa}$, which is approximately $3100$ times smaller than $\bar{E}_z$.

The shear modulus $\bar{\mu}_{yz}$ of the equivalent orthotropic plate is taken equal to the geometric mean of the Young's moduli in the two orthogonal directions [9].

$$\bar{\mu}_{yz} = \frac{\sqrt{\bar{E}_y \bar{E}_z}}{2} = 6.89 \times 10^7 \,\mathrm{N/m^2} \tag{4}$$

For the mass density $\bar{\rho}$, a value of $286.6\,\mathrm{kg/m^3}$ is chosen such that the equivalent plate has the same mass as the VL 603-K profile.

$$\bar{\rho}\bar{t} = m_\mathrm{w} = 113.5\,\mathrm{kg/m^2} \tag{5}$$

An overview of the model parameters can be found in Table 3.

| | $R$ [m] | $d$ [m] | $\bar{t}$ [m] | $\bar{E}_y$ [N/m$^2$] | $\bar{E}_z$ [N/m$^2$] | $\bar{\mu}_{yz}$ [N/m$^2$] | $\bar{\nu}_{yz}$ [-] | $\bar{\nu}_{zy}$ [-] | $\bar{\rho}$ [kg/m$^3$] |
|---|---|---|---|---|---|---|---|---|---|
| Model 1 | 5.60 | 12 | 0.396 | $2.47 \times 10^6$ | $7.68 \times 10^9$ | $6.89 \times 10^7$ | 0.0 | 0.0 | 286.6 |
| Model 2 | 5.60 | 18 | 0.396 | $2.47 \times 10^6$ | $7.68 \times 10^9$ | $6.89 \times 10^7$ | 0.0 | 0.0 | 286.6 |

Table 3: Geometric parameters and properties of the sheet piling wall used in the models

The sheet piling wall was modeled with 2-noded 2.5D orthotropic shell elements. These elements were coupled to a conforming BE mesh for the surrounding soil. The element dimensions were chosen to ensure at least eight elements per minimal shear wavelength.

### 3.3 Results for homogeneous halfspace

First, the effectiveness of a sheet piling wall as a mitigation measure and the influence of the orthotropic behavior is investigated. To facilitate the physical interpretation, the soil is assumed to be homogeneous in this section. The site at Horstwalde (Germany) with homogeneous soil conditions, which is one of the reference sites considered in the RIVAS project, is used. The soil characteristics of the Horstwalde site are given in Table 4.

| Layer | Thickness $h$ | Shear wave velocity $C_\mathrm{s}$ | Dilatational wave velocity $C_\mathrm{p}$ | Damping ratio $\beta$ | Density $\rho$ | Poisson's ratio $\nu$ |
|---|---|---|---|---|---|---|
| | $[\mathrm{m}]$ | $[\mathrm{m/s}]$ | $[\mathrm{m/s}]$ | [-] | $[\mathrm{kg/m^3}]$ | [-] |
| 1 | $\infty$ | 250 | 1470 | 0.025 | 1945 | 0.485 |

Table 4: Dynamic soil characteristics of the homogeneous halfspace (Horstwalde)

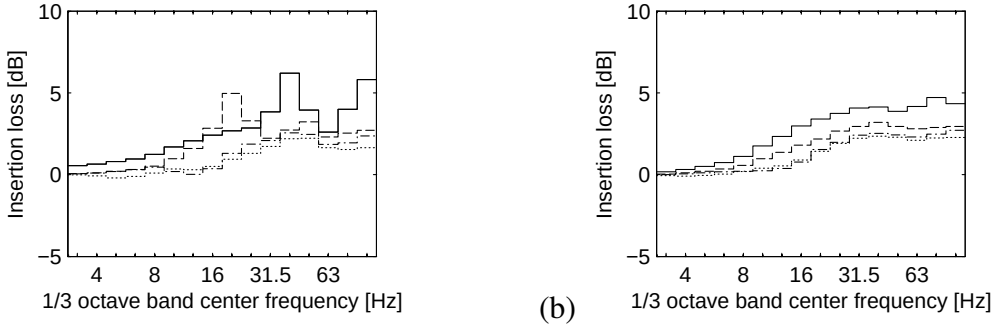


Figure 6: Vertical insertion loss at $8\,\mathrm{m}$ (solid line), $16\,\mathrm{m}$ (dashed line), $32\,\mathrm{m}$ (dash-dotted line) and $64\,\mathrm{m}$ (dotted line) for the $12\,\mathrm{m}$ deep sheet piling wall installed in the homogeneous halfspace. Excitation by (a) a point load and (b) a line load.

Figure 6 shows the vertical insertion loss in 1/3 octave bands for the $12\,\mathrm{m}$ deep sheet piling wall installed in the homogeneous halfspace, for several receiver points at the other side of the wall. The vertical insertion loss $\mathrm{IL_z}$ is the difference in vertical vibration levels in the case with and without vibration mitigation measure,

$$\mathrm{IL_z} = 20 \log_{10} \frac{|\hat{u}^{\mathrm{ref}}|}{|\hat{u}|},$$

where $\hat{u}$ is the vertical displacement in the case with mitigation measure and $\hat{u}^{\mathrm{ref}}$ is the vertical displacement in the reference case without mitigation measure. The hat denotes the representation in the frequency domain.

Figure 6a shows the insertion loss values when a vertical harmonic point force is applied to the soil at the surface at position $(x, y) = (0\,\mathrm{m}, 0\,\mathrm{m})$.

To simulate the efficiency of the sheet piling wall for train induced vibrations, the velocity response due to a number of uncorrelated forces applied at the line $x = 0\,\mathrm{m}$ (referred to as a line load in the following) and the corresponding insertion loss are also calculated. For the line load, the positions of the point forces are determined from the positions of the axles of an InterCity train, when the middle of the train is located at $y = 0\,\mathrm{m}$. The InterCity train consists of a locomotive HLE13, seven standard central HVI11 coaches and one back coach HV I11 BDx. It has a total length of $230.31\,\mathrm{m}$. The carriage length $L_\mathrm{t}$, the distance $L_\mathrm{b}$ between bogies and the axle distance $L_\mathrm{a}$ of all carriages are summarized in Table 5. The 1/3 octave band insertion loss values when the line load is applied, are shown in Figure 6b.

For the homogeneous halfspace, very little vibration reduction is seen below $12\,\mathrm{Hz}$. The frequency above which a reduction in vibration levels can be expected, is in the first place determined by the depth of the wall, relative to the Rayleigh wavelength. As a rule of thumb, it is stated that an open trench could reduce surface vibration propagation significantly at frequencies for which the ratio of the depth of the trench to the Rayleigh wave length of propagating vibration is larger than about $0.6$ [10]. As the Rayleigh wave velocity is $233\,\mathrm{m/s}$, a significant

| | Axles [-] | $L_\mathrm{t}$ [m] | $L_\mathrm{b}$ [m] | $L_a$ [m] |
|---|---|---|---|---|
| Locomotive HLE13 | 4 | 19.11 | 10.40 | 3.00 |
| Central coach HVI11 A | 4 | 26.40 | 18.40 | 2.56 |
| Central coach HVI11 B | 4 | 26.40 | 18.40 | 2.56 |
| End coach HV I11 BDx | 4 | 26.40 | 18.40 | 2.56 |

Table 5: The InterCity train

reduction can only be expected from $12\,\mathrm{Hz}$ on for an open trench with depth $12\,\mathrm{Hz}$. Therefore, the insertion loss for a sheet piling wall with the same depth will also be negligible below this frequency. Above $12\,\mathrm{Hz}$, the insertion loss of the sheet piling wall increases slowly to a plateau value which is reached at $30\,\mathrm{Hz}$. This plateau value depends on the distance from the point load. At the receiver position $x = 8\,\mathrm{m}$, which is located $2.4\,\mathrm{m}$ behind the wall, a value of $4\,\mathrm{dB}$ is reached. At $64\,\mathrm{m}$, the insertion loss at high frequencies is limited to $2\,\mathrm{dB}$.

At frequencies where the depth of the wall is large compared to the Rayleigh wavelength, the insertion loss will be determined by the reflection and transmission properties of the sheet pile wall. The difference in stiffness between the sheet piling wall and the soil will strongly determine the possible reduction in vibration levels. For the sheet piling wall, the bending stiffness along the vertical direction ($z$) is much larger than the bending stiffness along the longitudinal direction ($y$). Here, the influence of the orthotropy and the relative influence of the vertical and longitudinal stiffness is investigated by considering two cases (Table 6). In the first case, the sheet piling wall is modeled as an equivalent isotropic plate having the same bending stiffness in the longitudinal as in the vertical direction. In the second case, the longitudinal stiffness and mass of the sheet piling wall are set to zero.

| | $R$ [m] | $d$ [m] | $\bar{t}$ [m] | $\bar{E}_y$ [$\mathrm{N/m^2}$] | $\bar{E}_z$ [$\mathrm{N/m^2}$] | $\bar{\mu}_{yz}$ [$\mathrm{N/m^2}$] | $\bar{\nu}_{yz}$ [-] | $\bar{\nu}_{zy}$ [-] | $\bar{\rho}$ [$\mathrm{kg/m^3}$] |
|---|---|---|---|---|---|---|---|---|---|
| Case 1 | 5.60 | 12 | 0.396 | $6.99 \times 10^9$ | $6.99 \times 10^9$ | $2.69 \times 10^9$ | 0.3 | 0.3 | 286.6 |
| Case 2 | 5.60 | 12 | 0.396 | 0.0 | $7.68 \times 10^9$ | 0.0 | 0.0 | 0.0 | 0.0 |

Table 6: Geometric parameters and properties of the walls used to investigate the influence of the orthotropy and the relative influence of the vertical and longitudinal stiffness

Figure 7 shows the vertical insertion loss at $25\,\mathrm{Hz}$ for the sheet piling wall and the isotropic wall (case 1). At $25\,\mathrm{Hz}$, the sheet piling wall reduces the vibration levels at the surface with insertion loss values around $3\,\mathrm{dB}$. The reduction in vibration levels is fairly homogeneous at the surface behind the sheet piling wall. For the isotropic wall, the insertion loss at $25\,\mathrm{Hz}$ is larger than for the sheet piling wall in certain areas. On a line perpendicular to the wall, the insertion loss is similar as in the case of the sheet piling wall. Here, the longitudinal bending stiffness does not influence the vibration levels. The longitudinal bending stiffness does, however, influence the insertion loss noticeably for points further away from this line.

The wave impeding effect depends on the relationship between the Rayleigh wavelength in the soil and the free bending wavelength in the sheet piling wall [11]. The transmission of plane waves in the soil with a longitudinal wavelength smaller than the longitudinal bending wavelength is hindered. This is clear from Figure 8b which shows the insertion loss for case 1 in function of frequency and dimensional longitudinal wavenumber $\bar{k}_y = k_y C_s/\omega$. Superimposed

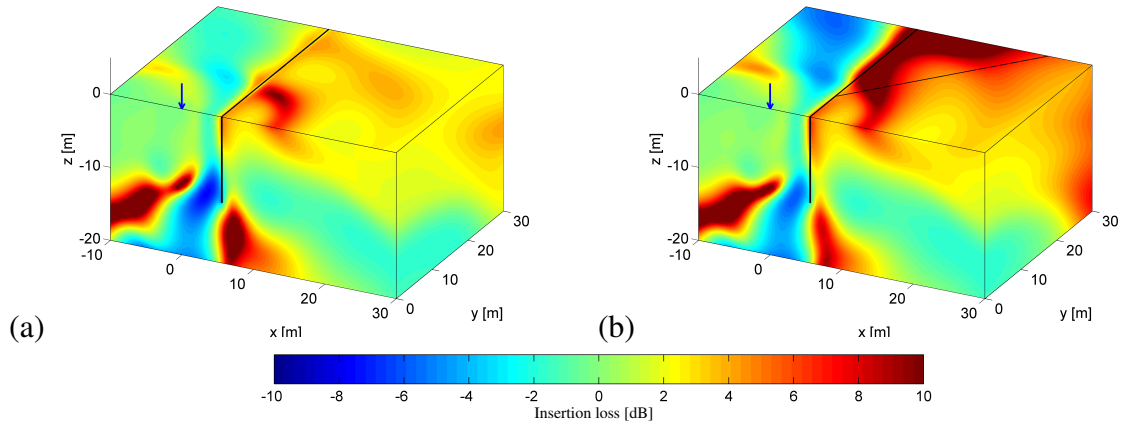


Figure 7: Vertical insertion loss for the sheet piling wall in the homogeneous halfspace at 25 Hz. (a) sheet piling wall and (b) case 1.

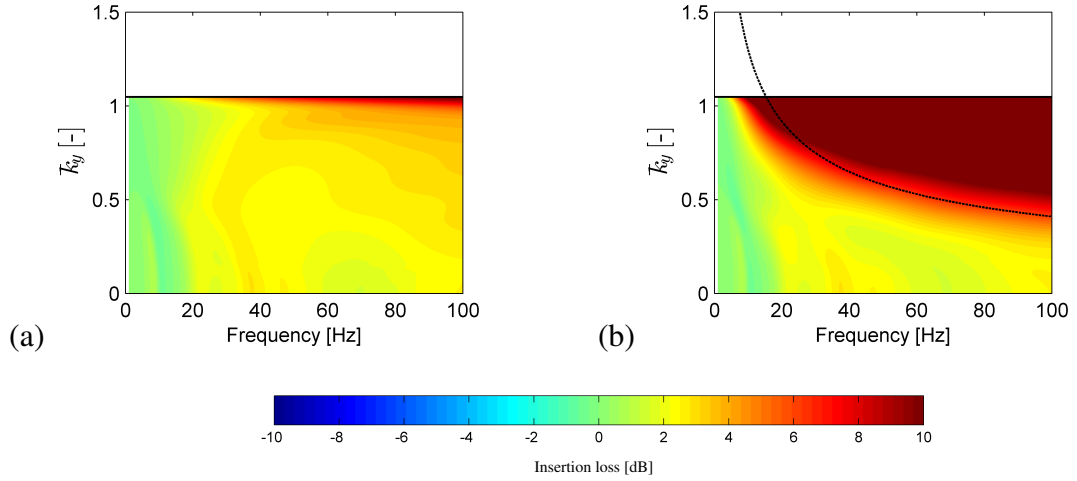


Figure 8: Vertical insertion loss $\mathrm{IL}_z$ ($x = 32\,\mathrm{m}$, $\overline{k}_y$, $\omega$, $z = 0\,\mathrm{m}$) for (a) the sheet piling wall and (b) case 1. Superimposed are the Rayleigh wave dispersion curve (solid black line) and the dispersion curve of a free bending wave in the wall in the longitudinal direction (dotted line).

is the dispersion curve of a Rayleigh wave propagating in the $y$-direction and the dispersion curve of a free bending wave in the longitudinal direction. Above a critical frequency, at which the Rayleigh wavelength in the soil is equal to the free bending wavelength in the wall, the isotropic wall starts to be effective as a wave impeding barrier. The critical frequency $f_c$ can be calculated from [9, 11]:

$$f_c = \frac{C_\mathrm{R}^2}{2\pi}\sqrt{\frac{\rho_\mathrm{w} A_\mathrm{w}}{E_{\mathrm{w},y} I_{\mathrm{w},y}}} \tag{6}$$

where $C_\mathrm{R}$ is the Rayleigh wave velocity of the soil. $\rho_\mathrm{w}$, $A_\mathrm{w}$, $E_{\mathrm{w},y}$ and $I_{\mathrm{w},y}$ are the density, the cross section area, the Young's modulus in the $y$-direction and the moment of inertia in the $y$-direction of the wall, respectively. For the isotropic wall (case 1), the critical frequency is equal to 15 Hz. This wave impeding effect caused by the longitudinal bending stiffness is not seen for the sheet piling wall (Figure 8a). The longitudinal bending stiffness is far too low, leading to a critical frequency of approximately 850 Hz.

The area for which a significant reduction of vibration levels is obtained above the critical

frequency, is determined by a critical angle $\theta_c$. The critical angle depends on the ratio between the free bending wavelength $\lambda_{\mathrm{b},y}$ in the wave barrier in the $y$-direction and the Rayleigh wavelength $\lambda_{\mathrm{R}}$ in the soil,

$$\theta_c = \sin^{-1}\left(\frac{\lambda_{\mathrm{R}}}{\lambda_{\mathrm{b},y}}\right) = \sin^{-1}\left(C_{\mathrm{R}}\sqrt[4]{\frac{\rho_{\mathrm{w}}A_{\mathrm{w}}}{E_{\mathrm{w},y}I_{\mathrm{w},y}\omega^2}}\right) \tag{7}$$

For the isotropic wall (case 1), the critical angle is equal to $51^\circ$ at $25\,\mathrm{Hz}$. This angle is also indicated on Figure 7b.

Figure 9 compares the 1/3 octave band insertion loss results of the sheet piling wall with the results for case 1 and case 2. The results are identical for the sheet piling wall model and case 2. This indicates that the reduction in vibration levels by the sheet piling wall is entirely due to the relatively high axial stiffness and vertical bending stiffness of the sheet piling wall. The effect of the longitudinal bending stiffness and the inertia of the sheet piling wall are negligible in the frequency range considered.

The vertical insertion loss values for a point load are similar for the orthotropic and isotropic wall model (case 1), especially at larger distances from the point load. For a point load, the vibration levels at a line perpendicular to the track are determined by Rayleigh waves which impinge perpendicularly on the sheet piling wall. At normal incidence, the longitudinal bending stiffness does not influence the vibrations in the sheet piling wall.

The insertion loss values for a line load differ strongly for the orthotropic and isotropic wall model. For the orthotropic sheet piling wall, the insertion loss for a line load is similar to the insertion loss for a point load. For the isotropic wall, the insertion loss for a line load is significantly larger than for a point load. The difference is larger for higher frequencies and for smaller distances from the sheet piling wall. This can be understood when looking at the results in Figure 7. For a line load, contributions from different point loads are added, which complies with a spatial averaging over the longitudinal direction.

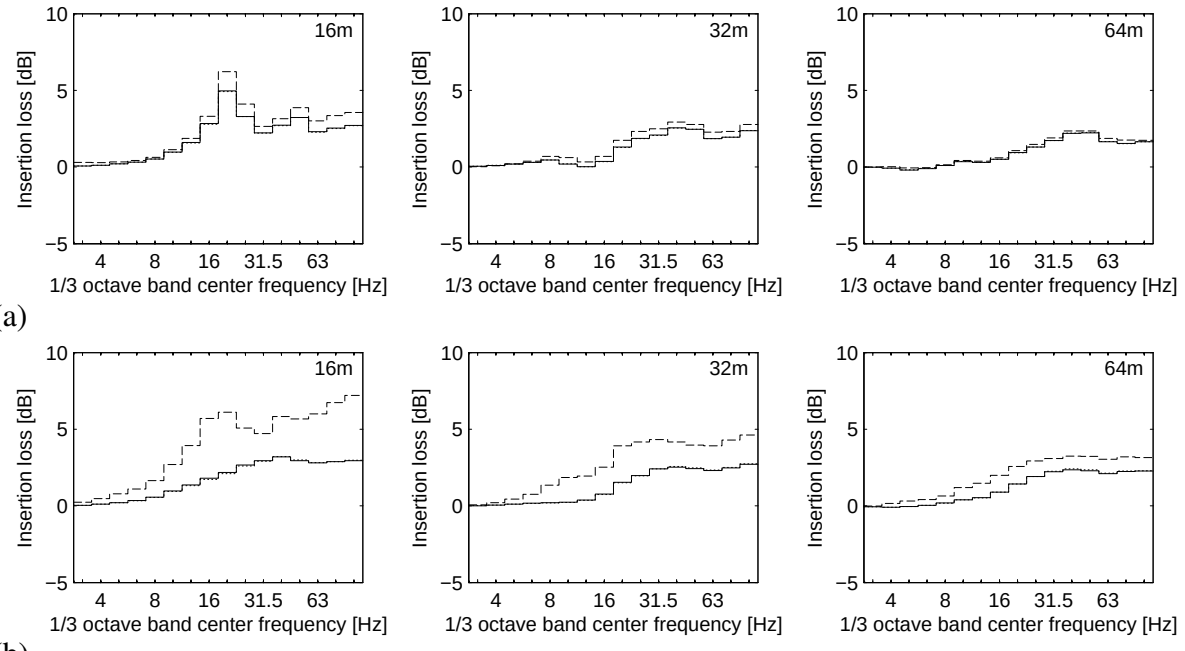


Figure 9: (a) Vertical insertion loss for a point load and (b) vertical insertion loss for a line load for the orthotropic sheet piling wall (solid lines), case 1 (dashed lines) and case 2 (dotted lines).

These results indicate that it is important to take into account the orthotropic behaviour of the sheet piling wall in the model. By use of an isotropic model for the sheet piling wall, the bending stiffness in the longitudinal direction is strongly overestimated. This will not affect the results for a point load at a line perpendicular to the track. The actual insertion loss for a train passage, here represented in a simplified way by a line load, will, however, be strongly overestimated.

### 3.4 Results for Furet test site

In this section, the efficiency of the sheet piling wall installed at the test site in Furet is analyzed. Separate 2.5D calculations have been made for depths of $12\,\mathrm{m}$ and $18\,\mathrm{m}$. In both models, the sheet pile wall is modeled as an equivalent orthotropic plate (Table 3). Calculations have been performed up to $50\,\mathrm{Hz}$ and $30\,\mathrm{Hz}$ for the $12\,\mathrm{m}$ and $18\,\mathrm{m}$ deep sheet pile wall, respectively.

Figure 10 shows the insertion loss at $5\,\mathrm{Hz}$ and $25\,\mathrm{Hz}$ for a vertical point load for the $12\,\mathrm{m}$ and $18\,\mathrm{m}$ deep sheet piling wall. At 5 Hz, the $12\,\mathrm{m}$ deep sheet piling wall only reduces the vibration levels significantly immediately behind the wall. At larger distances, the insertion loss is very limited. At $25\,\mathrm{Hz}$, the sheet piling wall reduces the vibration at the surface with more than $6\,\mathrm{dB}$. This reduction is reasonably homogeneous over the entire surface behind the sheet piling wall. It can be noticed, however, that the reduction in vibration levels is restricted to the top five meters of soil. Lines of constructive and destructive interference between direct and reflected Rayleigh waves can be observed at the other side of the sheet piling wall. For the $18\,\mathrm{m}$ deep sheet piling wall, a significant reduction is obtained at $5\,\mathrm{Hz}$ in the entire region behind the wall, although

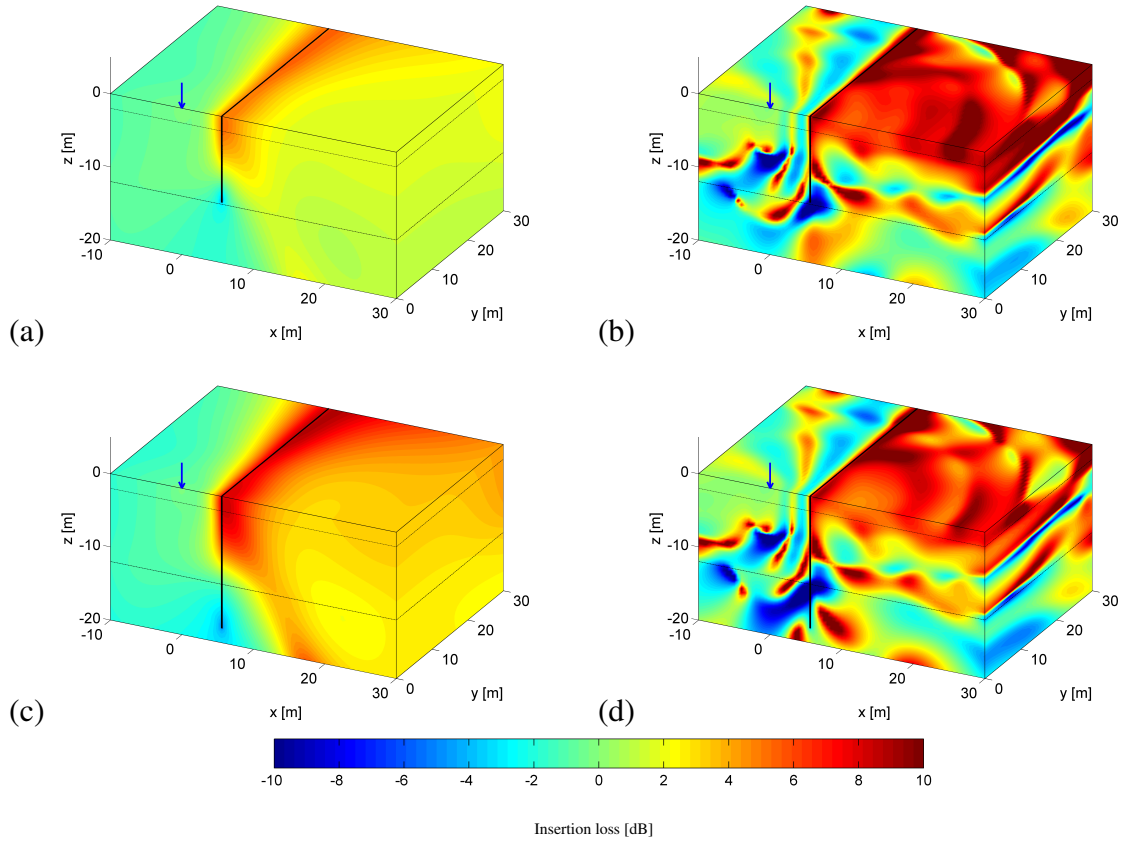


Figure 10: Vertical insertion loss for a vertical point load (a) at $5\,\mathrm{Hz}$, depth $12\,\mathrm{m}$, (b) at $25\,\mathrm{Hz}$, depth $12\,\mathrm{m}$, (c) at $5\,\mathrm{Hz}$, depth $18\,\mathrm{m}$ and (d) at $25\,\mathrm{Hz}$, depth $18\,\mathrm{m}$.

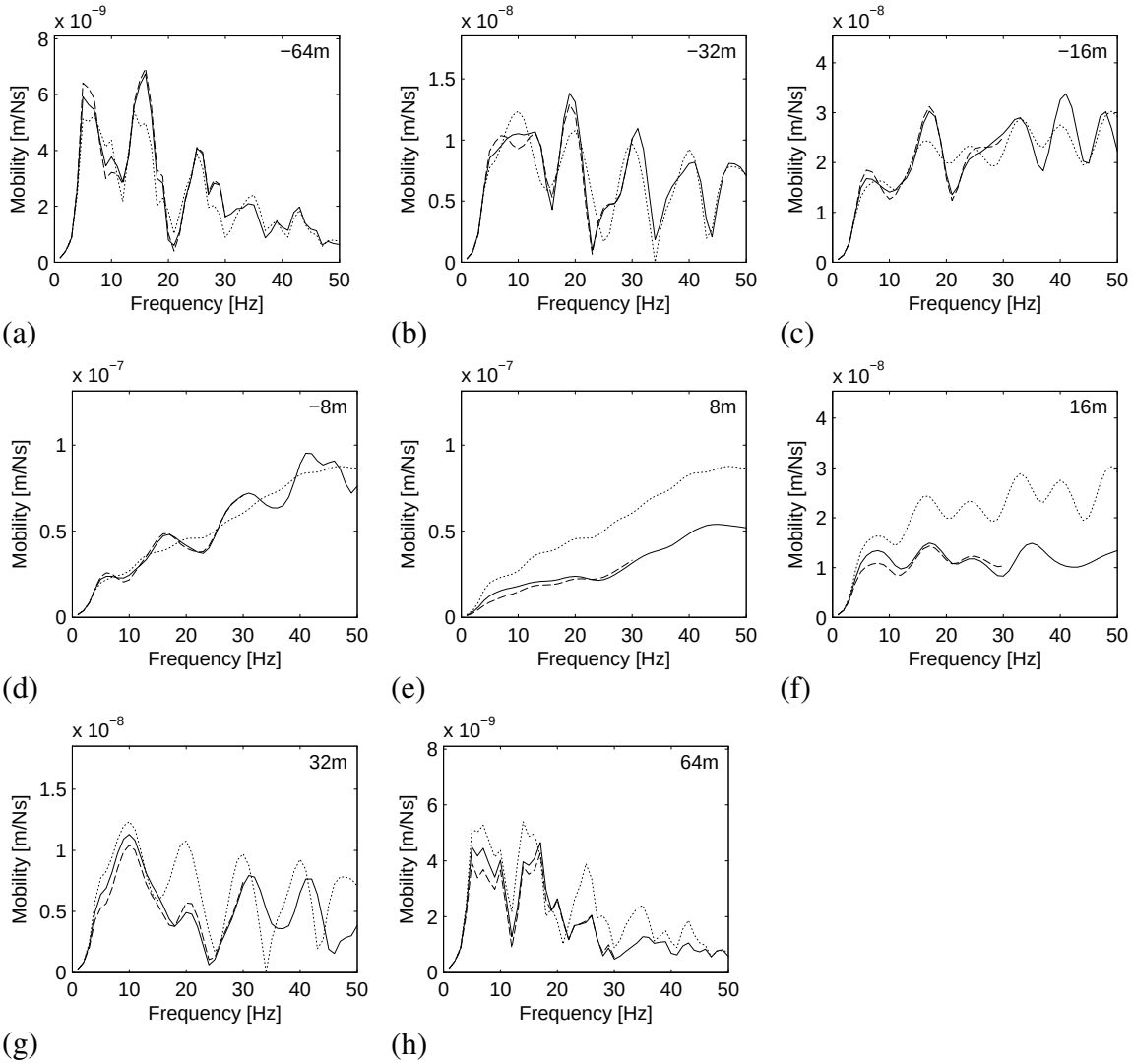


Figure 11: Transfer mobility at a distance of (a) $-64\,\mathrm{m}$, (b) $-32\,\mathrm{m}$, (c) $-16\,\mathrm{m}$, (d) $-8\,\mathrm{m}$, (e) $8\,\mathrm{m}$, (f) $16\,\mathrm{m}$, (g) $32\,\mathrm{m}$, and (h) $64\,\mathrm{m}$ from the point load in the reference case (dotted lines), for the $12\,\mathrm{m}$ deep (solid lines) and $18\,\mathrm{m}$ deep (dashed lines) sheet piling wall at the Furet test site.

the effectiveness decreases with increasing distance. The higher effectiveness compared with the $12\,\mathrm{m}$ deep sheet piling wall indicates that a significant amount of the vibrational energy passes underneath the $12\,\mathrm{m}$ deep wall at $5\,\mathrm{Hz}$. At $25\,\mathrm{Hz}$, the increased depth of the sheet piling wall does not significantly change the insertion loss. This may be explained by the fact that the motion of the Rayleigh waves is mainly limited to the top two layers at this frequency. Therefore, the insertion loss is largely determined by the transmission of vibrations through the sheet pile wall.

Figure 11 shows the transfer mobilities from a vertical harmonic point load applied to the soil at position $(x, y) = (0\,\mathrm{m}, 0\,\mathrm{m})$ to several positions in the free field for the Furet test site without mitigation measure, when the $12\,\mathrm{m}$ deep sheet piling wall is installed and when the $18\,\mathrm{m}$ deep sheet piling wall is installed. Figure 12 shows the corresponding insertion loss in 1/3 octave bands for the $12\,\mathrm{m}$ and $18\,\mathrm{m}$ deep sheet piling wall. Insertion loss values as measured with the RSMV at the test site are indicated with circles. The 1/3 octave band insertion loss values for the $12\,\mathrm{m}$ and $18\,\mathrm{m}$ deep sheet piling wall when the line load is applied, are shown in

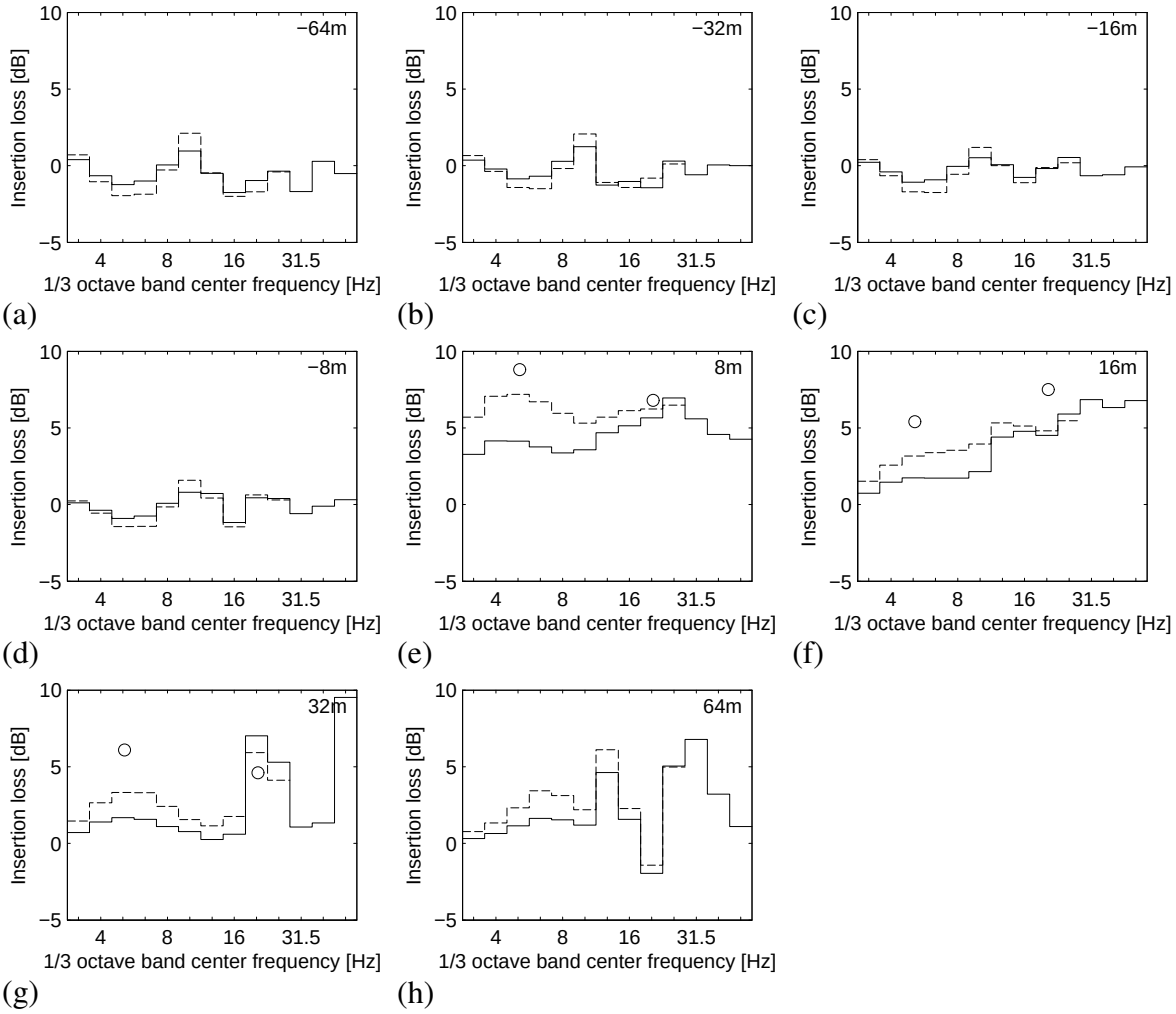


Figure 12: Vertical insertion loss at a distance of (a) $-64\,\mathrm{m}$, (b) $-32\,\mathrm{m}$, (c) $-16\,\mathrm{m}$, (d) $-8\,\mathrm{m}$, (e) $8\,\mathrm{m}$, (f) $16\,\mathrm{m}$, (g) $32\,\mathrm{m}$, and (h) $64\,\mathrm{m}$ in the case of a point load for the $12\,\mathrm{m}$ deep (solid lines) and $18\,\mathrm{m}$ deep (dashed lines) sheet piling wall at the Furet test site. Measured values with the RSMV are indicated with circles.

Figure 13.

For positions at the same side of the sheet piling wall as the point load ($-64\,\mathrm{m}$, $-32\,\mathrm{m}$, $-16\,\mathrm{m}$, $-8\,\mathrm{m}$), the vibration levels are either increased or reduced due to constructive or destructive interference of the direct and reflected waves (Figure 11). As a result, the insertion loss for the point load varies on average between plus and minus $2\,\mathrm{dB}$ (Figure 12). The insertion loss for a line load is smoothed (Figure 13), as the calculation involves a spatial averaging of the vibration field. For the line load, the vibration levels are on average increased by $2\,\mathrm{dB}$ at these positions due to the presence of the sheet pile of wall. For the $18\,\mathrm{m}$ deep sheet piling wall, the increase in vibration levels is about $1\,\mathrm{dB}$ larger at frequencies below $10\,\mathrm{Hz}$.

The results for receiver points at the other side of the sheet piling wall ($8\,\mathrm{m}$, $16\,\mathrm{m}$, $32\,\mathrm{m}$, $64\,\mathrm{m}$) indicate that the sheet piling wall can effectively reduce the vibration levels. For a point load, insertion loss values of $5\,\mathrm{dB}$ and more are predicted above $20\,\mathrm{Hz}$ for the $12\,\mathrm{m}$ deep sheet piling wall (Figure 12). It must be reminded, however, that the frequency range $4-5\,\mathrm{Hz}$ is targeted. Below $20\,\mathrm{Hz}$, the insertion loss is limited to $2\,\mathrm{dB}$ for the $12\,\mathrm{m}$ deep wall. Only for small distances behind the wall ($8\,\mathrm{m}$), the insertion loss can reach up to $4\,\mathrm{dB}$ below $10\,\mathrm{Hz}$. For a line load, the insertion loss is on average $1$ to $2\,\mathrm{dB}$ larger (Figure 13). The results indicate

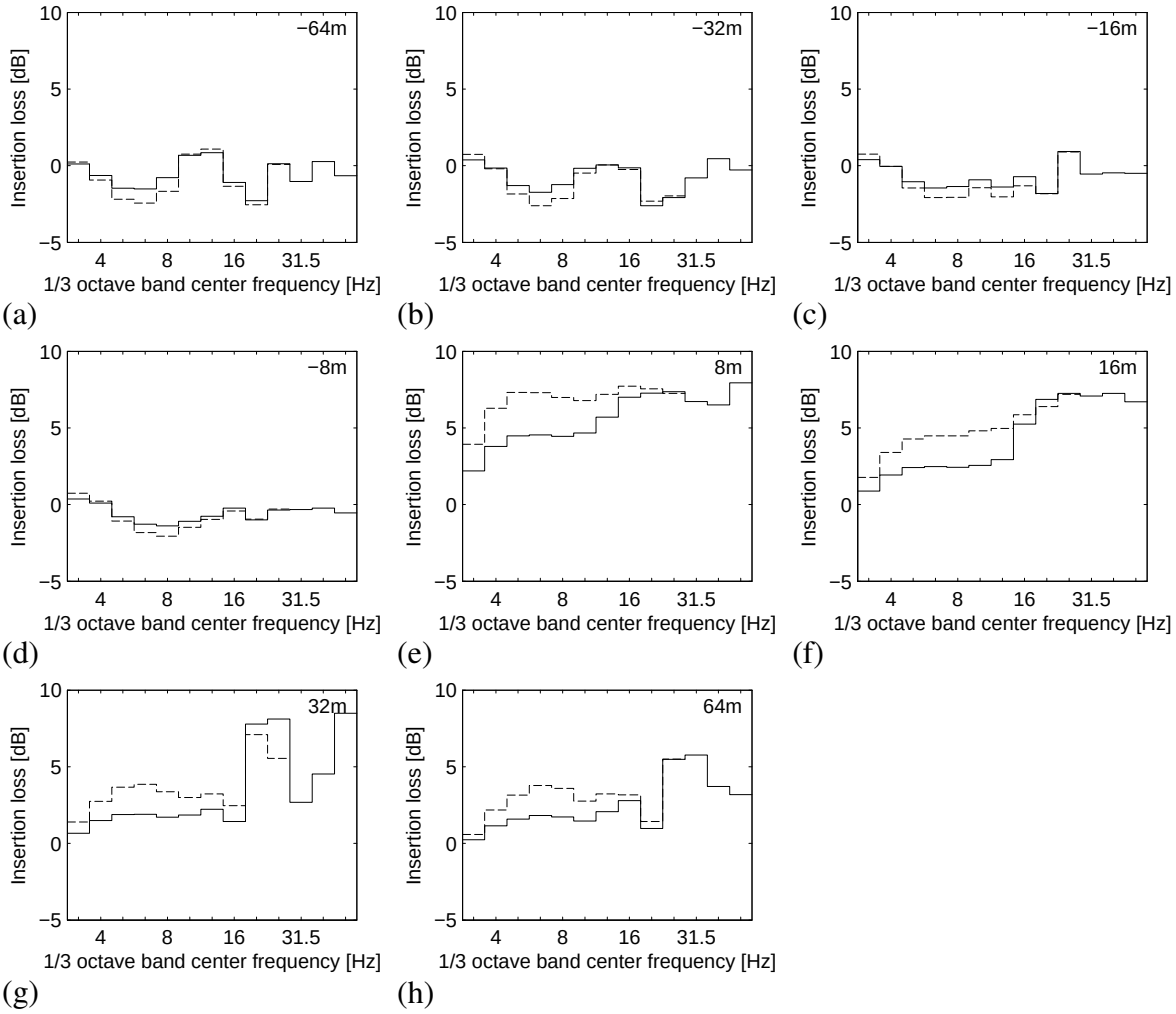


Figure 13: Vertical insertion loss at a distance of (a) $-64\,\mathrm{m}$, (b) $-32\,\mathrm{m}$, (c) $-16\,\mathrm{m}$, (d) $-8\,\mathrm{m}$, (e) $8\,\mathrm{m}$, (f) $16\,\mathrm{m}$, (g) $32\,\mathrm{m}$, and (h) $64\,\mathrm{m}$ in the case of a line load for the $12\,\mathrm{m}$ deep (solid lines) and $18\,\mathrm{m}$ deep (dashed lines) sheet piling wall at the Furet test site.

that the increase in depth to $18\,\mathrm{m}$ has a favorable effect at low frequencies. The insertion loss is increased by $2\,\mathrm{dB}$ in the 1/3 octave bands between $4\,\mathrm{Hz}$ and $16\,\mathrm{Hz}$, both for a point load and a line load. Above $20\,\mathrm{Hz}$, the insertion loss is not improved. Prediction results even indicate a slight reduction in efficiency for the deeper wall. For the actually constructed sheet piling wall with alternating depth, the insertion loss is expected to lie in between the values for a $12\,\mathrm{m}$ deep and an $18\,\mathrm{m}$ deep sheet piling wall.

A preliminary comparison with the experimental results is made in Figure 12. Although the order of magnitude of the insertion loss is reasonably well predicted, further processing of the measurements is needed before a detailed comparison can be made and possible reasons for discrepancies can be investigated.

## 4 CONCLUSIONS

To reduce the train induced vibrations at the site of Furet, a sheet piling wall was installed next to the track. The depth of the sheet piles is 12 m with every fourth pile extended to $18\,\mathrm{m}$. The effectiveness of the sheet pile wall was analyzed by means of 2.5D calculations for a $12\,\mathrm{m}$

and $18\,\mathrm{m}$ deep wall. An equivalent orthotropic plate model of the sheet pile wall was adopted.

The sheet piling wall acts as a stiff wave barrier, of which the effectiveness is determined by the depth and the contrast in stiffness between the barrier and the soil. The sheet piling wall only starts to act when the depth of the sheet piling wall is sufficiently large compared to the Rayleigh wavelength in the soil. Increasing the depth from 12 m to 18 m consequently results in an increased reduction at low frequencies.

It is important to take into account the orthotropic behavior of the sheet piling wall, as the bending stiffness in the vertical direction (along the profiles) is much larger than the bending stiffness in the longitudinal direction (perpendicular to the profiles). Calculations show that the reduction of vibration levels is entirely due to the relatively high axial stiffness and vertical bending stiffness, while the longitudinal bending stiffness is too low to affect the transmission of vibrations. A simplified isotropic model does not allow accounting accurately for the transmission of waves at grazing incidence.

Calculation results for the site of Furet show that at $8\,\mathrm{m}$ from the track, a reduction in transmitted ground vibration is already obtained at frequencies above $4\,\mathrm{Hz}$. The performance decreases with increasing distance from the track as observed in the vibration measurements carried out for train passages and with the RSMV. Further processing of the measurements is needed before a detailed comparison to the numerical results can be made.

## 5 ACKNOWLEDGEMENTS

The results presented in this paper have been obtained within the frame of the EU FP 7 project RIVAS (Railway Induced Vibration Abatement Solutions).

## REFERENCES

[1] D. Stiebel, B. Nelain, and N. Vincent. How to measure and transfer efficiencies of vibration-mitigation measures: results of the European project RIVAS, P. Sas, D. Moens, and S. Jonckheere eds. *Proceedings of ISMA 2012 International Conference on Noise and Vibration Engineering*, pages 2959–2971, Leuven, Belgium, September 2012. CD-ROM.

[2] D. Aubry, D. Clouteau, and G. Bonnet, Modelling of wave propagation due to fixed or mobile dynamic sources. N. Chouw and G. Schmid eds. *Workshop Wave '94, Wave propagation and Reduction of Vibrations*, pages 109–121, Ruhr Universität Bochum, Germany, December 1994.

[3] X. Sheng, C.J.C. Jones, and M. Petyt, Ground vibration generated by a harmonic load acting on a railway track. *Journal of Sound and Vibration*, **225**(1), 3–28, 1999.

[4] G. Lombaert, G. Degrande, and D. Clouteau, Numerical modelling of free field traffic induced vibrations. *Soil Dynamics and Earthquake Engineering*, **19**(7), 473–488, 2000.

[5] L. Andersen and S.R.K. Nielsen, Reduction of ground vibration by means of barriers or soil improvement along a railway track. *Soil Dynamics and Earthquake Engineering*, **25**, 701–716, 2005.

[6] S. François, M. Schevenels, G. Lombaert, P. Galvín, and G. Degrande, A 2.5D coupled FE-BE methodology for the dynamic interaction between longitudinally invariant structures and a layered halfspace. *Computer Methods in Applied Mechanics and Engineering*, **199**(23-24), 1536–1548, 2010.

[7] M. Schevenels, G. Degrande, and S. François, EDT: an ElastoDynamics Toolbox for Matlab. *Book of Abstracts of the Inaugural International Conference of the Engineering Mechanics Institute (EM08)*, page 82, Minneapolis, Minnesota, U.S.A., May 2008.

[8] M. Schevenels, S. François, and G. Degrande, EDT: An ElastoDynamics Toolbox for MATLAB. *Computers & Geosciences*, **35**(8), 1752–1754, 2009.

[9] C. Hopkins, *Sound insulation*, Elsevier Ltd., Oxford, 2007.

[10] C.J.C. Jones, D.J. Thompson, and J.I. Andreu-Medina, Initial theoretical study of reducing surface-propagating vibration from trains using earthworks close to the track. *Proceedings of the 8th International Conference on Structural Dynamics, EURODYN 2011*, pages 684–691, Leuven, Belgium, July 2011.

[11] P. Coulier, S. François, G. Degrande, and G. Lombaert, Subgrade stiffening next to the track as a wave impeding barrier for railway induced vibrations. *Soil Dynamics and Earthquake Engineering*, 2013. http://dx.doi.org/10.1016/j.soildyn.2012.12.009i. In press.